Int. J. Electron. Commun. (AEÜ) 123 (2020) 153320

Contents lists available at ScienceDirect

International Journal of Electronics and Communications (AEÜ)

journal homepage: www.elsevier.com/locate/aeue

Regular paper

Multilayered additive-manufactured half-wavelength coupled line filters

Héctor García-Martínez [a,*], Ernesto Ávila-Navarro [a], Germán Torregrosa-Penalva [b], Enrique Bronchalo [b], Carolina Blanco-Angulo [a], Maurizio Bozzi [c]

[a] Materials Science Department, Optical and Electronic Technology, University Miguel Hernández of Elche, 03202 Elche, Spain
[b] Communication Engineering Department, University Miguel Hernández of Elche, 03202 Elche, Spain
[c] Department of Electrical, Computer, and Biomedical Engineering, University of Pavia, 27100 Pavia, Italy

ARTICLE INFO

Article history:
Received 17 March 2020
Accepted 17 June 2020

Keywords:
Additive manufacturing
Coupling coefficient
Multilayered filter
3D printing

ABSTRACT

This work presents the design, fabrication and measurements of third-order multilayered filters by additive manufacturing technology. The filters are fabricated using conventional half-wavelength line resonators and a low-cost 3d polylactic acid polymer additive manufacturing process, which allows rapid prototyping and fabrication of complex topologies. The designs, performed at a centre frequency of 2.0 GHz, aim to provide fast manufacturing and get enhanced performances when compared to conventional coupled line third order filters using microstrip technology on commercial substrates. The simulated and measured responses of the fabricated prototypes are in all cases in good agreement.

1. Introduction

Nowadays, additive manufacturing techniques are employed in a wide variety of fields, including for example medicine, civil engineering, aeronautics and satellites construction [1]. This technology is starting to be used in other contexts thanks to the emergence of new and promising materials coupled to the cost reduction and better performing features of 3D printers [2,3]. In the particular area of radiofrequency and microwave devices, additive manufacturing has been mainly exploited to implement metallic waveguide structures and aperture antennas whose construction following traditional mechanical procedures is normally too expensive. In these cases, a 3D additive manufactured structure is normally first fabricated using a plastic material which is then metallized, thus reducing both the cost and weight of the fabricated device [4–12].

Commercial substrates with given physical and electrical characteristics are traditionally used for the implementation of microwave planar circuits, where a range of transmission line technologies are employed including microstrip lines, striplines, coplanar waveguides or, more recently, substrate integrated waveguides (SIW). Microwave circuit designers choose the appropriate substrate for the fabrication of their device, so that the size of the resulting circuit and its electrical performance meets some particular requirements. Throughout the designing process the substrate remains a constant parameter that can be only modified during the very first stages of the designing process.

Additive manufacturing does allow the characteristics of the substrate material to become part of the designing process of microwave planar devices [13,14]. The substrate geometrical and electrical characteristics can be optimized as it is done with the rest of the dimensions of the circuit. Moreover, additive manufacturing techniques can be used to attain circuit topologies and geometries that cannot be achieved when standard commercial laminates are used, allowing a faster and simpler prototyping process. Additionally, 3D manufacturing constitutes an inexpensive alternative to technologies like LTCC [15]. For example, in [16] different multilayer filter topologies are fabricated using a varnish to separate the conductive elements, in [17] an EBG (electromagnetic band gap) transmission line including a varying height profile is presented and in [18] SIW structures are fabricated using additive manufacturing techniques. This, in turn, can lead to the attainment of enhanced electrical characteristics. On the other hand, two relevant drawbacks of this technology have to be addressed in order to reach satisfactory designs: inability of polylactic acid polymer (PLA) materials to cope with high temperatures and the metallization procedure on plastic materials.

In order to demonstrate some of the advantages stated before, in this work we present the design of several third order simple multilayered pass-band filters operating at 2.0 GHz. They are implemented by means of three conventional half-wavelength

* Corresponding author.
E-mail addresses: mhector@umh.es (H. García-Martínez), evila@umh.es (E. Ávila-Navarro), gtorregrosa@umh.es (G. Torregrosa-Penalva), ebronchalo@umh.es (E. Bronchalo), cblanco@umh.es (C. Blanco-Angulo), maurizio.bozzi@unipv.it (M. Bozzi).

https://doi.org/10.1016/j.aeue.2020.153320
1434-8411/

resonators to achieve improved performances when compared to the same designs fabricated in microstrip technology on a commercial substrate [19]. In particular, we have focused in the study of three different features: maximum pass-band bandwidth, harmonic suppression response and introduction of additional cross-coupling transmission zeros in the filter response.

The work is organized as follows: Section 2 describes the additive manufacturing process and PLA material electrical characterization, Section 3 introduces the filter topology and the calculations of the input/output quality factors and coupling coefficients between resonators. Subsequently, Section 4 presents the different filter designs, and some final conclusions are given in Section 5.

2. Additive manufacturing process

For the fabrication of the prototypes, a 3D printer BQ Hephestos was used together with a 1.75 mm diameter PLA filament. The filling pattern density in each layer can be modified from 100% to 15% (structures with less density material are too weak to provide an adequate consistency) [20]. Fig. 1 shows the multilayer structure implemented for the different filter prototypes. The top (PLA − 3) and bottom (PLA − 1) PLA layers are 0.4 mm high, while the middle layer (PLA − 2) has a height of $n \times 0.1$ mm. The density filling pattern of all PLA layers is 100%. Once the bottom PLA 0.4 mm layer is fabricated an intermediate metallic layer (metal − 1) is placed on top. Metallic layers are fabricated by gluing a 0.035 mm high copper sheet to the PLA structure, using a commercial non-conductive 2216B/A epoxy adhesive. The different resonators in each metallic layer are fabricated using a Protomat S42 LPKF milling machine. Then, the middle PLA layer (PLA − 2) is produced and the second metallic layer (metal − 2) glued on top and milled. Finally, the top PLA layer (PLA − 3) is printed and the whole structure is enclosed by the top and bottom glued metallic ground planes.

On the other hand, in order to implement the multilayer filter prototypes, it is necessary to know the electrical characteristics of the PLA. This PLA component is a multipurpose material, not intended specifically for high frequency applications. Its characterization yielded a relative dielectric permittivity of ε_r = 2.88 at 2.0 GHz and a loss tangent of tan δ = 0.02 (for a 100% density filling pattern) [13].

3. Filter topology and coupling coefficients

The third order filters are fabricated making use of conventional half-wavelength line resonators. In all cases the resonators have a width w = 0.63 mm, which corresponds to the 50 Ω transmission line shown in Fig. 1b. The coupling coefficient [21] between two resonators under different geometries has been obtained using the expression

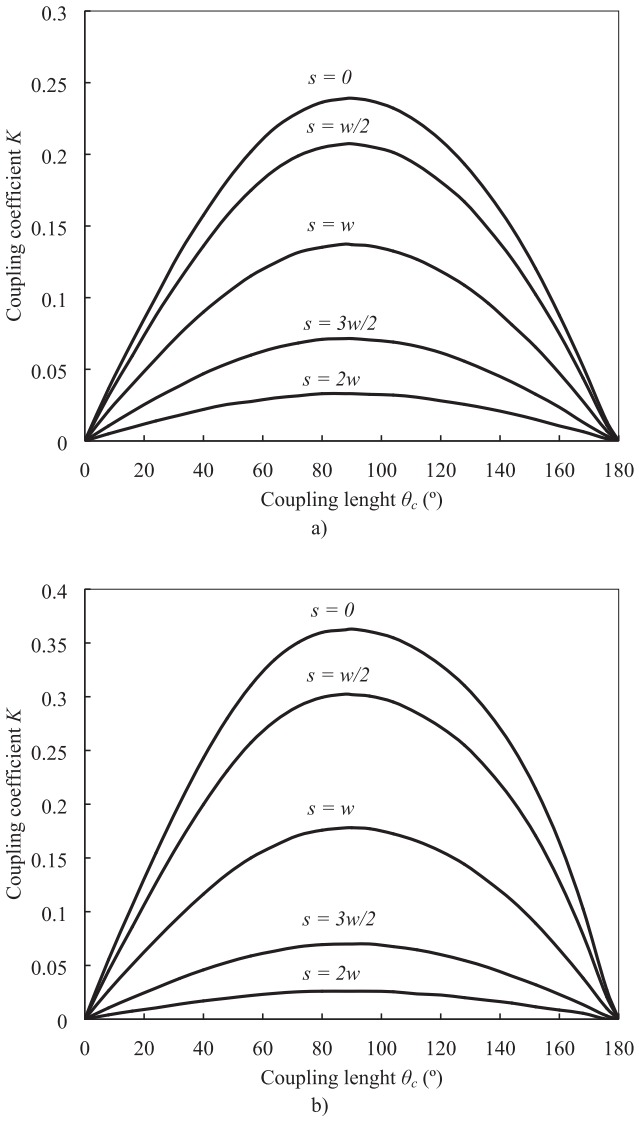

Fig. 2. Coupling coefficient of two half-wavelength line resonators as a function of the coupling length θ_c, for different values of the transversal spacing s between resonators. (a) PLA − 2 intermediate layer is 0.4 mm high. (b) PLA − 2 intermediate layer is 0.2 mm high.

$$K = \frac{f_{p1}^2 - f_{p2}^2}{f_{p1}^2 + f_{p2}^2} \tag{1}$$

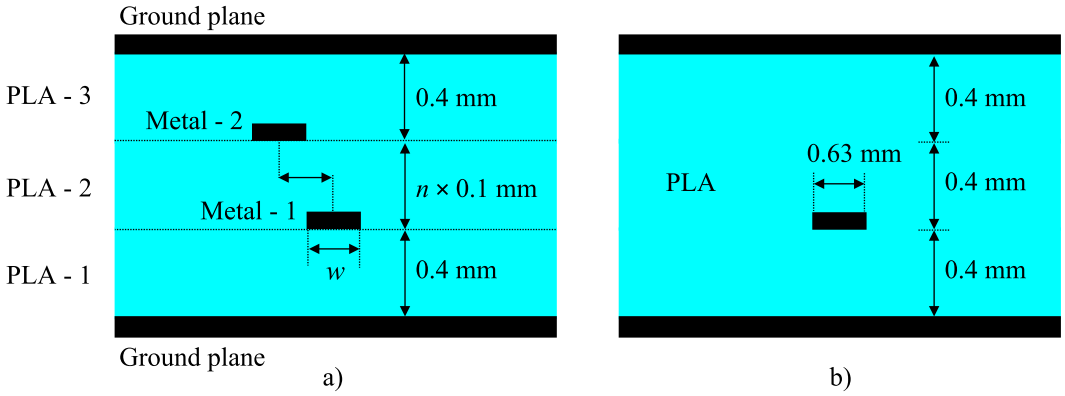

Fig. 1. Cross-section of the multilayer structures. Dark regions are 0.035 mm high copper conductors. (a) 2 resonator structure. (b) 50 Ω transmission line.

where f_{p1} and f_{p2} are the natural resonant frequencies of the coupling configuration. These frequencies are determined by means of electromagnetic simulation using software ADS by Keysight for a weak input/output coupling of the coupled resonators structure.

The coupling coefficient for the structure shown in Fig. 1 has been computed for different values of the relative transversal separation s between the half-wavelength resonators as a function of the coupling section length θ_c. These results are given in Fig. 2a and Fig. 2b. As it can be seen in Fig. 2b the maximum coupling coefficient is approximately twice the one obtained for two coupled line resonators separated 0.2 mm in microstrip technology [19]. This fact is exploited for obtaining enhanced wideband filter responses. Another important fact to be pointed out is that the shape of these coupling coefficients follows a sinusoidal behaviour of the form $K(\theta_c) \propto \sin \theta_c$, corresponding to the TEM nature of the structure of Fig. 1 [21].

4. Pass-band multilayer filter designs with different configurations

In this section, several filter designs are presented. The filters exhibit a third order Chebyshev response, centered at 2.0 GHz and with a 0.1 dB ripple 10% fractional bandwidth (*FBW*). The low-pass prototype elements are: $g_0 = g_4 = 1$, $g_1 = g_3 = 1.0316$ and finally $g_2 = 1.1474$. The design parameters for the filters are calculated using [21]

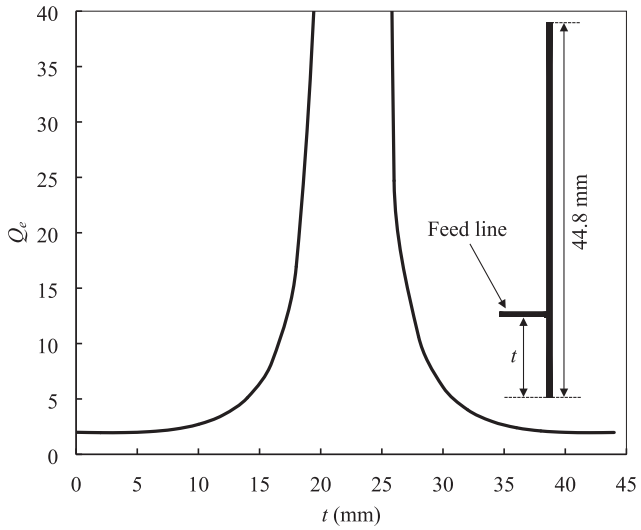

Fig. 3. Simulated external quality factor Q_e as a function of the position t of the feed line. PLA – 2 intermediate layer is 0.4 mm high.

$$Q_{ei} = Q_{eo} = \frac{g_0 g_1}{FBW} \tag{2}$$

$$K_{12} = K_{23} = \frac{FBW}{\sqrt{g_1 g_2}} \tag{3}$$

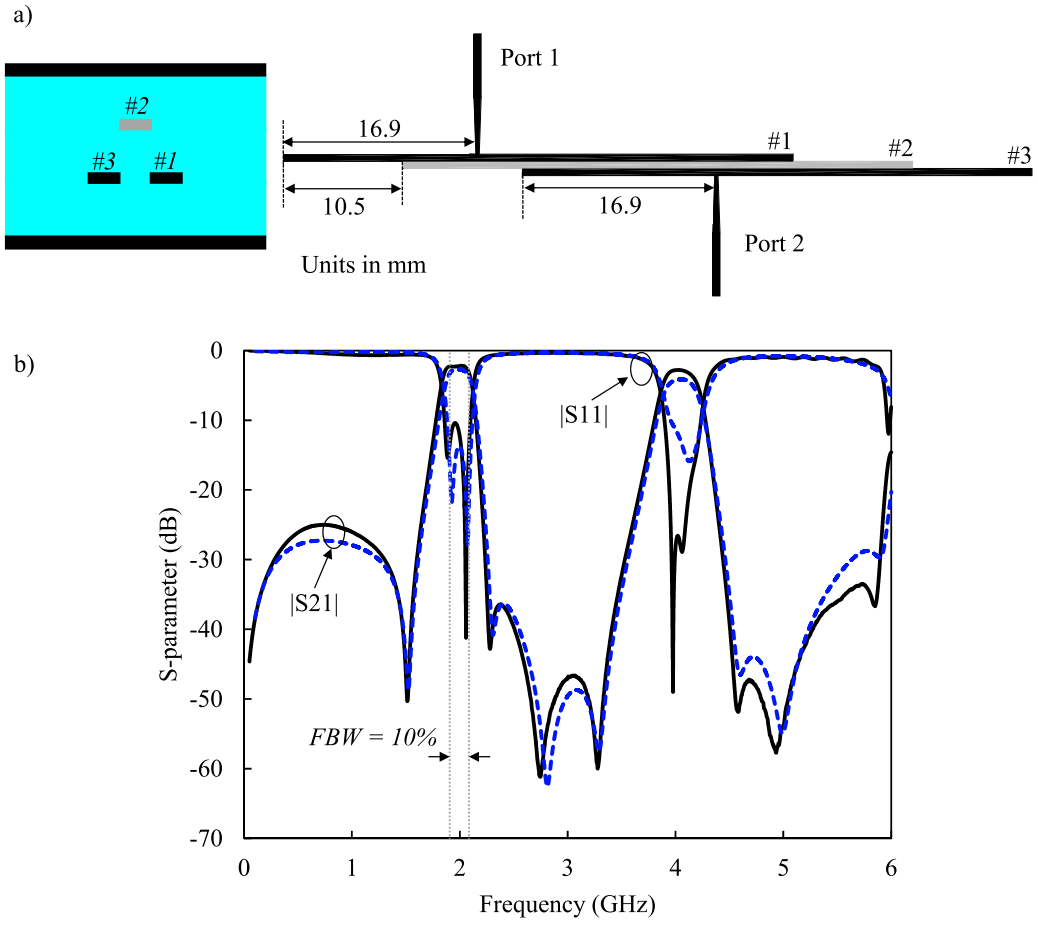

Fig. 4. (a) Filter dimensions to scale in mm, and cross-section filter diagram. (b) Measured (black continuous line) and simulated (blue dashed line) S-parameters. (For interpretation of the references to colour in this figure legend, the reader is referred to the web version of this article.)

where K_{ii+1} is the coupling coefficient between resonators i and $i+1$, and Q_{ei} and Q_{eo} are the input and output external quality factors. The feeding line position t controls the external quality factor as it is shown in Fig. 3. [21] (electromagnetic simulations were carried out using the structure of Fig. 1b).

4.1. Conventional 10% relative bandwidth filter design

The first filter aims to demonstrate the feasibility of the technology, through a structure that exhibits a relative bandwidth of $FBW = 10.0\%$. For this design, using (2) and (3) gives $Q_{ei} = Q_{eo} = 10.316$ and $K_{12} = K_{23} = 0.092$ [22]. The filter is formed by three resonators. Input resonator (#1) and output resonator (#3) are on the same middle bottom metal – 1 layer. Resonator #2 is on the middle top metal – 2 layer (shown in grey colour in Fig. 4a). The dimensions of the filter are also given in Fig. 4a. In this case the PLA - 2 intermediate layer is 0.4 mm high and $s = w$ was chosen. The required coupling coefficient was obtained accordingly from Fig. 2a with $\theta_c = 138°$. Different resonator configurations are possible to achieve the desired band-pass performance, but the one fabricated provided an appropriate out-of-band response due to the inclusion of different transmission zeros. Scattering parameter filter measurements were carried out using Agilent Technologies a E8363B vector network analyser (with 3201 number of points, range frequency 0.1–6 GHz and IF filter bandwidth 10 KHz). The measured response is compared to the simulated S-parameters in Fig. 4b. The measured insertion loss in the pass-band (including SMA connector losses) is less than 1.3 dB, while both sets of curves are in good agreement. The filter occupies a circuit area of 65.8 × 1.89 mm^2, which corresponds to $0.73\lambda_0 \times 0.02\lambda_0$, where

Fig. 5. Photograph of the fabricated filter before its implementation is completed. On top of the structure resonator #2 can be clearly seen.

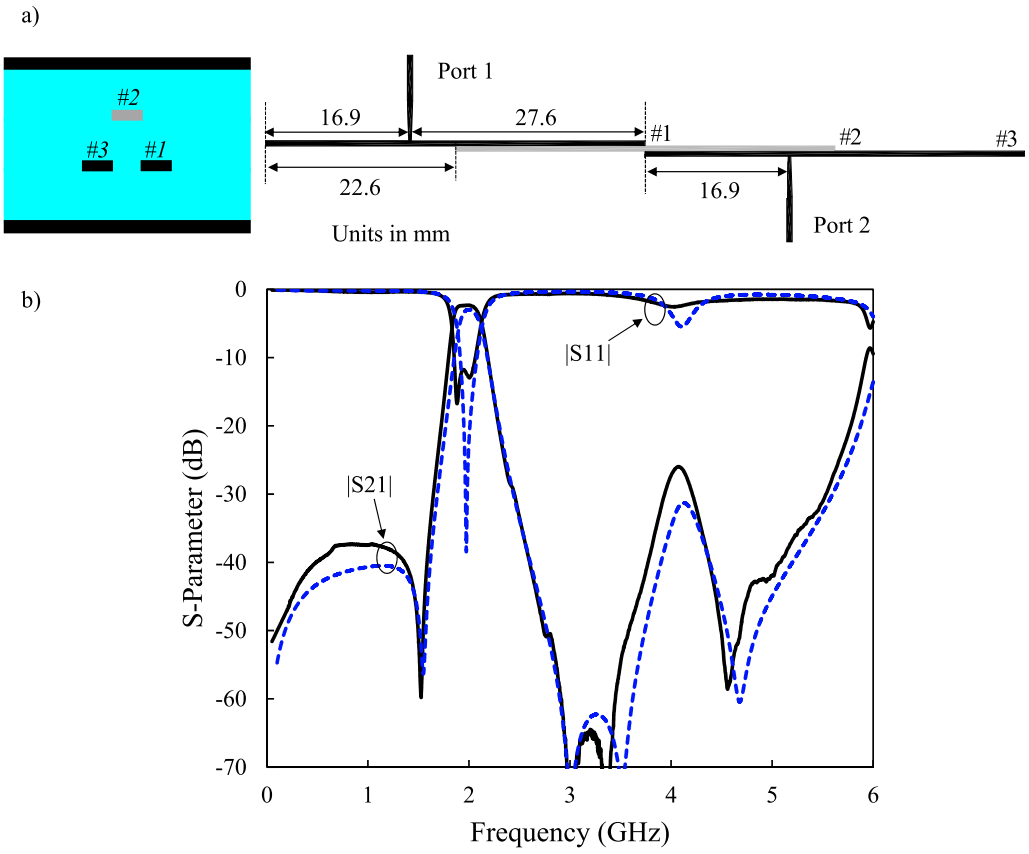

Fig. 6. (a) Filter dimensions to scale in mm, and cross-section filter diagram. PLA – 2 middle layer is in this filter 0.8 mm high. (b) Measured (black continuous line) and simulated (blue dashed line) S-parameters. (For interpretation of the references to colour in this figure legend, the reader is referred to the web version of this article.)

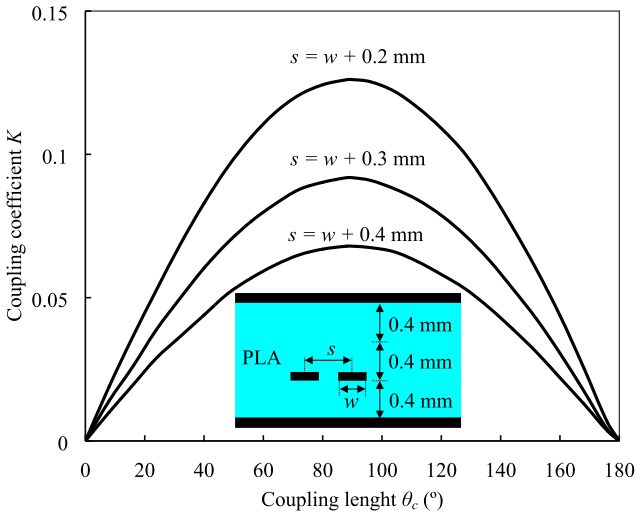

Fig. 7. Coupling coefficient of two half-wavelength line resonators as a function of the coupling section length, for different values of the transversal spacing s between resonators (w = 0.63 mm). Both resonators are on the metal – 1 layer, while PLA – 2 intermediate layer is 0.4 mm high.

λ_0 is the guided wavelength of the 50 Ω transmission line at 2.0 GHz shown in Fig. 1b. Three transmission zeros can be seen near the pass-band, which provide a high selectivity. The first transmission zero at 1.51 GHz results from the feeding position point in port #2, where a virtual ground appears when $t \approx \lambda/4$. The second transmission zero at 2.28 GHz is produced by cross-coupling effect, since there is some coupling between the first and third resonators. The third transmission zero at 2.8 GHz results from the feeding position point in port #1, where a virtual ground appears when $t \approx \lambda/4$.

A picture of the implemented filter before the fabrication process is finished is shown in Fig. 5. In this picture the top PLA – 3 layer, as well as the metallic top and bottom ground planes, vias and connectors are not included.

4.2. Harmonic suppression filter design

The second filter aims to improve the out-of-band response, by suppressing the pass-band at $2f_0$. In order to improve the performance of the previous design, the separation between resonators was kept $s = w$, and the height of the PLA – 2 intermediate layer was modified to give $K_{12} = K_{23} = 0.092$ for a coupling length $\theta_c = 90°$. This coupling length guarantees a null coupling coefficient between resonators at $2f_0$, due to the TEM behaviour of the structure. Thus the harmonic spurious pass-band around 4.0 GHz in Fig. 4b can be suppressed.

The dimensions and disposition of the different resonators are also shown in Fig. 6a. The measured response is compared to the simulated S-parameters in Fig. 6b. Measured transmission losses in the pass-band are in this case 2.3 dB (including SMA connectors), while again both sets of curves are in good agreement. The harmonic spurious pass-band at 4.0 GHz is suppressed by more than 25.0 dB. Although other alternatives are possible, the implementation carried out for the filter is not symmetric. This is done

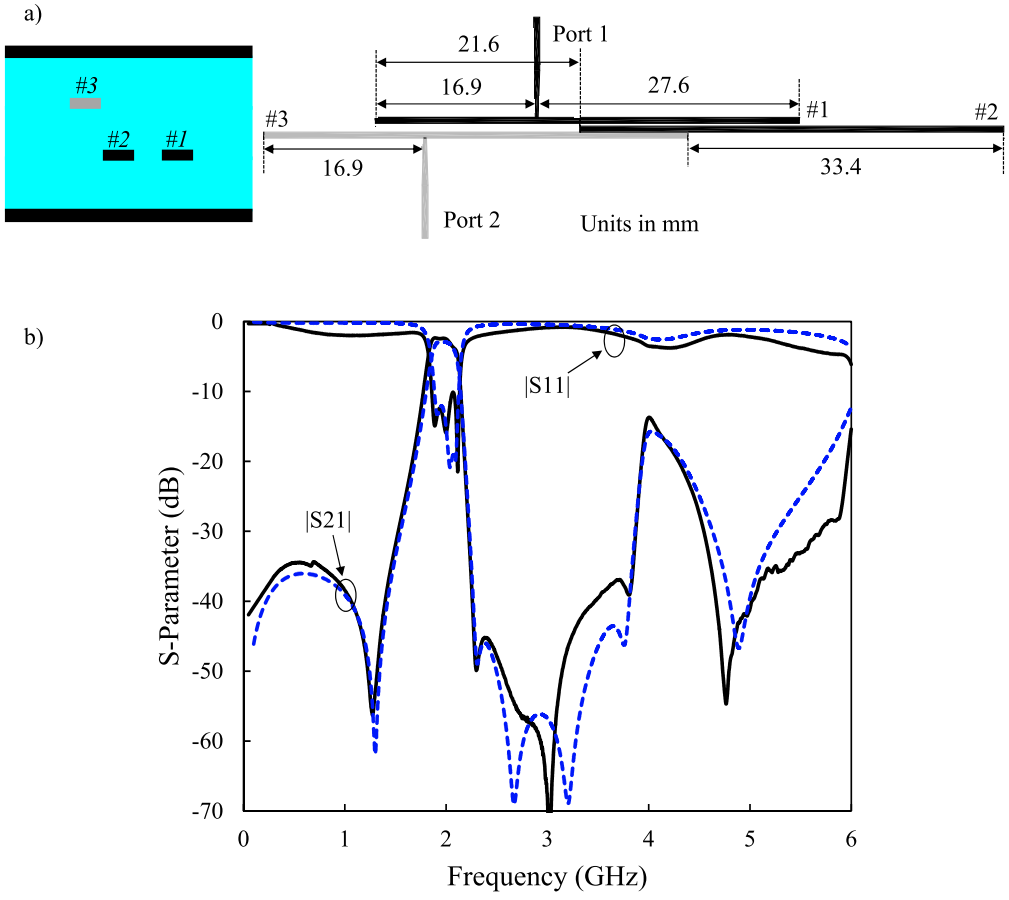

Fig. 8. (a) Filter dimensions and cross-section filter diagram where resonators #1 and #2 are on the same metal – 1 layer. (b) Measured (black continuous line) and simulated (blue dashed line) S-parameters. (For interpretation of the references to colour in this figure legend, the reader is referred to the web version of this article.)

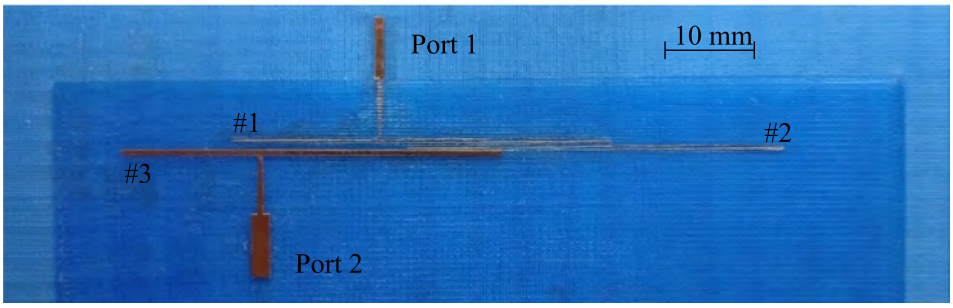

Fig. 9. Photograph of the fabricated filter before the manufacturing process is completed.

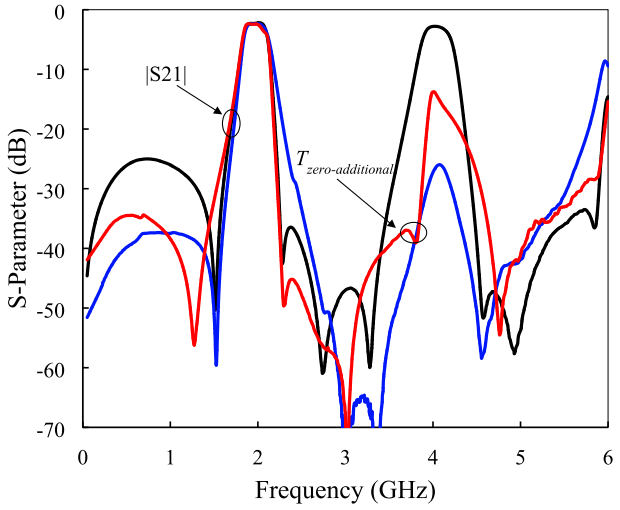

Fig. 10. Comparison of the three filters implemented for different resonator configurations. Conventional filter (black continuous line), harmonic suppression filter (blue continuous line) and introduction of additional transmission zeros (red continuous line). (For interpretation of the references to colour in this figure legend, the reader is referred to the web version of this article.)

in order to take advantage of two different transmission zeros produced by the quarter wavelength open ended stubs in resonators #1 and #3 seen from the feeding lines. The filter occupies a circuit area of 89.6 × 1.89 mm^2, which corresponds to $\lambda_0 \times 0.02\lambda_0$, where λ_0 is the guided wavelength of a 50 Ω transmission line at 2.0 GHz.

4.3. Introduction of additional transmission zeros filter design

The third filter adopts a modified topology, with the aim to introduce additional transmission zeros. The filter response presented in the previous subsection can be further improved if the disposition of the resonators is modified. One alternative consists in placing resonators #1 and #2 on the same metallic layer (metal −1) and resonator #3 on a different metallic layer (metal − 2). Fig. 7 shows the coupling coefficient between two resonators when both are on the same layer as a function of the coupling section length θ_c. The magnitude of the values obtained resembles those of a pair of coupled half-wavelength resonators in conventional microstrip technology [19].

The designed filter parameters are similar to those calculated in Section 4.1. All three resonators are again 0.63 mm wide, $s = w + 0.3$ mm has been chosen between resonators #1 and #2 (which leads to a coupling length section between these two resonators of $\theta_c = 90°$), while $s = 0$ mm is chosen between resonators #2 and #3 (leading to a coupling length section of $\theta_c = 44°$). The dimensions and disposition of the different resonators are also shown in Fig. 8a. Measured and simulated S-parameters are compared in Fig. 8b. Measured transmission losses in the pass-band are 2.5 dB, while both sets of curves are again in good agreement. The filter occupies a circuit area of 77.8 × 2.19 mm^2, which corresponds to $0.87\lambda_0 \times 0.024\lambda_0$, where λ_0 is the guided wavelength of a 50 Ω transmission line at 2.0 GHz. The coupling coefficient at the second harmonic ($2f_0$) is $K = 0$, because $\theta_c = 180°$ at $2f_0$ ($\theta_c = 90°$ at f_0). Therefore, no spurious band is obtained at $2f_0$ since it is cancelled by the transmission zero produced by the null coupling. In this design a more selective response is attained by the introduction of an additional transmission zero at 2.3 GHz due to cross-coupling between resonators #1 and #3. On the other side the spurious harmonic response at 4.0 GHz is attenuated 15 dB.

A picture of the implemented filter before the fabrication process is finished is shown in Fig. 9. In this picture resonator #3 on top of the multilayer structure can be clearly seen, as well as the fact that ports #1 and #2 are in different layers.

The measured response of the three filters implemented for different resonator configurations is shown in Fig. 10. In the case of the third design there is an additional transmission zero produced by cross-coupling between resonator #1 and resonator #3.

4.4. Maximum bandwidth filter design

In the fourth filter the main goal is to implement a filter with the largest possible bandwidth at the design frequency $f_0 = 2.0$ GHz. The low-pass filter prototype elements are those given at the beginning of Section 4. The maximum achievable coupling factor provided by the proposed structure, $K = 0.36$ as shown in Fig. 3b, is employed to yield from (3) $FBW = 39\%$ and from (2) $Q_{ei} = Q_{eo} = 2.62$. The PLA − 2 intermediate layer between resonators #1 and #3 and resonator #2 is in this case 0.2 mm high.

This configuration provides a −3dB fractional bandwidth close to 70% for the filter design with maximum bandwidth (similar designs with the same constraints in microstrip technology, using commercial laminates, yield fractional bandwidths close to 35%) [19]. In order to get the desired coupling coefficient, the coupling length between resonators is $\theta_c = 96°$ for $s = 0$, see Fig. 2b, while the appropriate external quality factors are obtained for $t \approx 9$ mm, as shown in Fig. 3.

The dimensions and disposition of the different resonators are also shown in Fig. 11a. The measured response is compared to the simulated S-parameters in Fig. 11b. Measured transmission losses in the pass-band are 0.9 dB, while both sets of curves are again in good agreement. The filter occupies a circuit area of 88.9 × 0.63 mm^2, which corresponds to $\lambda_0 \times 0.007\lambda_0$, where λ_0 is the guided wavelength of a 50 Ω transmission line at 2.0 GHz. The coupling coefficient at the second harmonic ($2f_0$) is $K = 0$, because $\theta_c = 180°$ at $2f_0$ ($\theta_c = 90°$ at f_0). Therefore, no spurious band is obtained at $2f_0$ since it is cancelled by the transmission zero produced by the null coupling. Small changes in the filter center frequency response might be due to deviations in the final filter dimensions and in the relative dielectric permittivity.

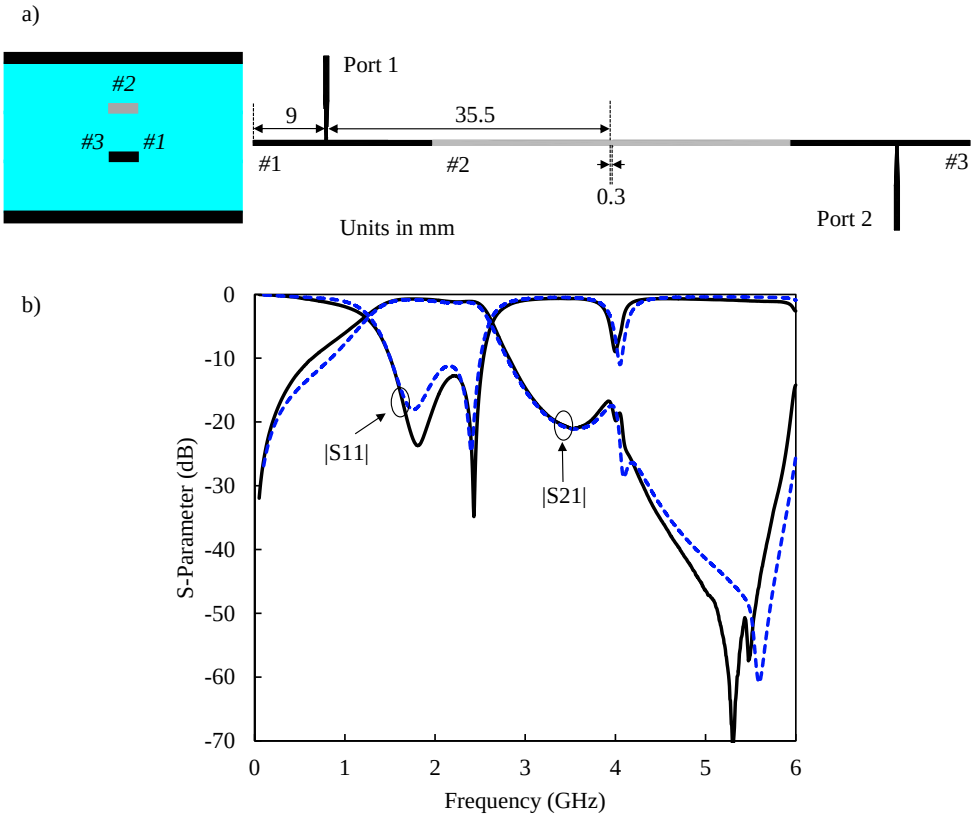

Fig. 11. (a) Filter dimensions, and cross-section filter diagram, where resonators #1 and #3 are aligned. (b) Measured (black continuous line) and simulated (blue dashed line) S-parameters. (cambiar).

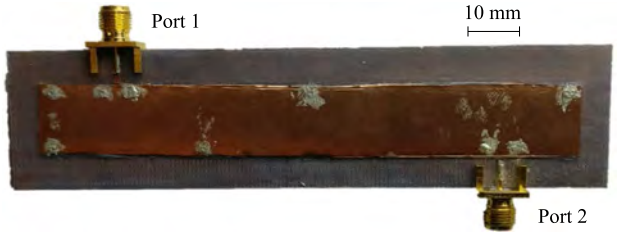

Fig. 12. Photograph of the final fabricated filter after the manufacturing process is completed.

Table 1
Technology performance comparison.

Technology	Insertion loss (dB)	Maximum fractional bandwidth (FBW)	Harmonic suppression (dB)	Filter shape factor (−30 dB)
Conventional microstrip design [19]	1.3	35%	17	3.0
Multilayer additive manufacturing, this work	2.3	70%	25	2.3

The picture of the final filter is shown in Fig. 12, which includes SMA connectors and vias. To improve the electrical contact between the SMA connectors and the tracks, a conductive silver epoxy RS PRO that cures at room temperature has been used.

Table 1 compares the performance characteristics of the different filter configurations implemented in conventional microstrip technology and using additive manufacturing techniques.

5. Conclusions

In this work, conventional low cost 3D additive manufacturing techniques have been used for the implementation of several half-wavelength resonator multilayer filters. Multilayer configurations allow the achievement of larger coupling coefficients in comparison to those obtained making use of standard microstrip technology on commercial laminates and demonstrate the simplicity and speed of creating these configurations using a 3D printer. The designed filters exhibit enhanced characteristics, such as suppression of the spurious harmonic pass-band, up to 70% pass-band fractional bandwidth and cross-coupling transmission zeros for better selectivity, and the measured filter responses are in good agreement with electromagnetic simulations.

Declaration of Competing Interest

The authors declare that they have no known competing financial interests or personal relationships that could have appeared to influence the work reported in this paper.

Appendix A. Supplementary material

Supplementary data to this article can be found online at https://doi.org/10.1016/j.aeue.2020.153320.

References

[1] Gao W, Zhang Y, Ramanujana D, Ramani K, Chen Y, Williams CB, et al. The status, challenges, and future of additive manufacturing in engineering. Comput Aided Des 2015;69:65–89.

[2] Kim C, Espalin D, Liang M, Xin H, Cuaron A, Varela I, et al. 3d printed electronics with high performance, multi-layered electrical interconnect. IEEE Access 2018;5. pp. 25 286–25 294.

[3] Flowers PF, Reyes C, Ye S, Kim MJ, Wiley BJ. 3d printing electronic components and circuits with conductive thermoplastic filament. Addit Manuf 2017;18:156–63.

[4] Kyovtorov V, Georgiev I, Margenov S, Stoychev D, Oliveri F, Tarchi D. New antenna design approach - 3D polymer printing and metallization. experimental test at 14–18GHz. AEU - Int J Electron Commun 2017;73:119–28.

[5] Massoni E, Silvestri L, Alaimo G, Marconi S, Bozzi M, Perregrini L, et al. 3-d printed substrate integrated slab waveguide for single-mode bandwidth enhancement. IEEE Microw Wireless Compon Lett 2017;27:536–8.

[6] Addamo G, Peverini OA, Manfredi D, Calignano F, Paonessa F, Virone G, et al. Additive manufacturing of ka-band dual-polarization waveguide components. IEEE Trans Microw Theory Techn 2018;66:3589–96.

[7] Pons-Abenza A, García-Barceló JM, Romera-Pérez A, Alvarez-Melcon A, Quesada-Pereira FD, Hinojosa-Jiménez J, et al. Design and implementation of evanescent mode waveguide filters using dielectrics and additive manufacturing techniques. AEU - Int J Electron Commun 2020;116.

[8] Goh GL, Ma J, Chua KLF, Shweta A, Yeong WY, Zhang YP. Inkjet-printed patch antenna emitter for wireless communication application. Virtual Phys Prototyp 2016;11(4):289–94.

[9] Mirzaee M, Noghanian S, Wiest L, Chang I. Developing flexible 3D printed antenna using conductive ABS materials. In: IEEE international symposium on antennas and propagation & USNC/URSI national radio science meeting, Vancouver, Canada, July. 2015 p. 1308–9.

[10] Guan-Long H, Shi-Gang Z, Tan-Huat C, Tat-Soon Y. 3-D metal-direct-printed wideband and high-efficiency waveguide-fed antenna array. In: IEEE MTT-S international microwave symposium, Phoenix, United States, May. 2015. p. 1–4.

[11] Agarwala S, Yeong WY. Aerosol jet fabricated biodegradable antenna for bioelectronics application. Trans Addit Manuf Meets Med 2019;1.

[12] Francis V, Jain PK. 3D printed polymer dielectric substrates with enhanced permittivity by nanoclay inclusion. Virtual Phys Prototyp 2017;12:107–15.

[13] García-Martínez H., Torregrosa-Penalva G., Ávila-Navarro E., Coves-Soler Á., Bronchalo E. Complex structures in microwave circuits by using additive manufacturing techniques. In: Proc. 49th Eur. Microw. Conf. (EuMC), Paris, France, Oct. 2019. p. 782–5, doi: 10.23919/EuMC.2019.8910748.

[14] Moscato S, Bahr R, Le T, Pasian M, Bozzi M, Perregrini L, et al. Infill dependent 3D-printed material based on NinjaFlex filament for antenna applications. IEEE Antennas Wirel Propag Lett 2016;15(1):1506–9.

[15] Feng W, Gao X, Che W, Yang W, Xue Q. LTCC Wideband bandpass filters with high performance using coupled lines with open/shorted stubs. IEEE Trans Compon Packag Manuf Technol 2017;7(4):602–9.

[16] Bouazzaoui H, Donnart K, Manchec A, Quendo C, Allanic R, Karpus F, et al. Ultra-wideband bandpass low-cost multilayer technologies filter using varnish. In: Proc. 48th Eur. Microw. Conf. (EuMC), Madrid, Spain, Sep. 2018. p. 687–90.

[17] Hester J, Nguyen E, Tice J, Radisic V. A novel 3d-printing-enabled 'roller coaster' transmission line. In: 2017 IEEE international symposium on antennas and propagation, USNC-URSI national radio science meeting, San Diego, USA, Jul. 2017.

[18] Moscato S, Bahr R, Le T, Pasian M, Bozzi M, Perregrini L, et al. Additive manufacturing of 3d substrate integrated waveguide components. IET Electron Lett 2015;51(18):124–6.

[19] Sanchez-Soriano MA, Bronchalo E, Torregrosa-Penalva G. Parallel coupled line filter design from an energetic coupling approach. IET Microwaves Antennas Propag 2011;5:568–75.

[20] García-Martínez H, Ávila-Navarro E, Torregrosa-Penalva G, Rodriguez-Martínez A, de la Casa-Lillo M. Analysis of microwave passive circuits designed using 3D printing techniques. Elektronika ir Elektrotechnika 2019;25(2):36–9.

[21] Hong J-S, Lancaster MJ. Microstrip filters for RF/microwave applications. New York, USA: John Wiley and Sons Inc; 2001.

[22] Pozar DM. Microwave engineering. New York, USA: John Wiley and Sons Inc; 1998.